Nuclear Instruments and Methods in Physics Research A248 (1986) 118–129
North-Holland, Amsterdam

AEROGEL CHERENKOV COUNTERS AT DESY

Günter POELZ

II. Institut für Experimentalphysik der Universität Hamburg, FRG

The production of aerogels of silica with indices of refraction between $n = 1.011$ and 1.026 was investigated at DESY to improve the optical quality of the material and to equip the Cherenkov system of the TASSO detector. Transmission lengths of $\Lambda = 5$ cm for blue light were obtained for tiles with $n = 1.025$. The absorption length in the visible spectrum ranges from 1 to 10 m. In Cherenkov counters with aerogel of $n = 1.025$ up to 10 photoelectrons can be expected. The Cherenkov system of TASSO subtends a cross section of about 12 m^2. It is equiped with aerogel of $n = 1.024$. The light yield for relativistic particles was 4 photoelectrons at the beginning. A decrease by 0.5 yr^{-1} is observed

1. Introduction

In high energy physics it is common to identify a charged particle and its kinematical parameters by the measurement of its momentum and its velocity. Cherenkov detectors have developed into a standard tool because they operate in the $\gamma = (1 - \beta^2)^{-1/2}$ range from about 1 to 100 which is not easily accessible by other devices. Pions, kaons and protons in present high energy experiments reach energies of several GeV. Threshold Cherenkov detectors for these particles need indices of refraction below 1.1 which are often produced with gases under high pressure. The design for chambers operating in this region was drastically simplified when porous materials serving as Cherenkov radiators [1,2] were invented. These chambers complement the time-of-flight counters, which cover the low energy region. Aerogel of silica is up to now the only porous substance with sufficient optical transparency. Its quality has been improved substantially in recent times [3] so that large size detectors can be constructed [4].

2. Production and properties of silica aerogel

Aerogel is a material of high porosity with a microstructure smaller than the wavelength of visible light. Therefore, its index of refraction n is lower than that of solid silica. It increases linearly with the density ρ of the gel (in g/cm^3), similar to that for gases as shown in fig. 1, by

$$n - 1 = 0.21 \cdot \rho. \qquad (1)$$

Microphotographs of pulverized aerogel (fig. 2), taken with a transmission electron-microscope [6], show that the solid consists of grains with a diameter smaller than 10 nm. This is consistent with gas desorption measurements [7] from which a diameter of 4 nm can be derived via the size of the internal surface. On the other hand, photographs (fig. 3) of the surface of a fragment taken with a scanning microscope [5,8] show spheres with diameters of about 50 nm. These are probably clusters of the small grains. The volume of solid silica in aerogel with a typical density of 0.13 g/cm^3 is 6% of the total. Such a loose packing is obtained if the particles are arranged [9] with a coordination number of 3, i.e. each particle touches 3 other ones. Such an arrangement is depicted by the model [10] in fig. 4. One infers from this model that the diameter of the pores should be about 200 to 280 nm. Gaps of such a size are also seen in fig. 3.

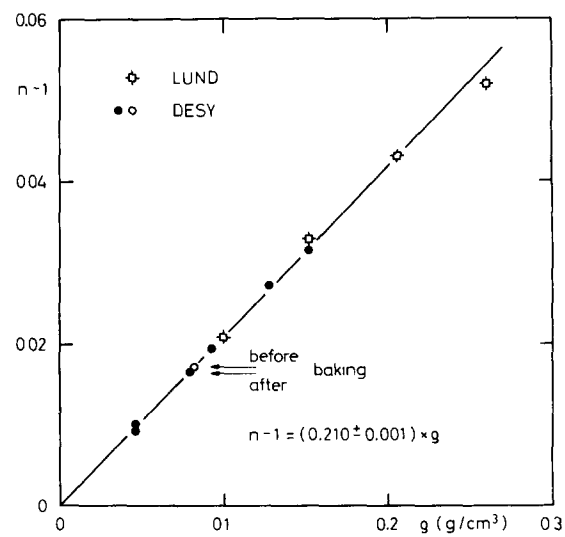

Fig. 1. Relation between refractivity and density of silica aerogel manufactured at DESY and Lund [5].

0168-9002/86/$03.50

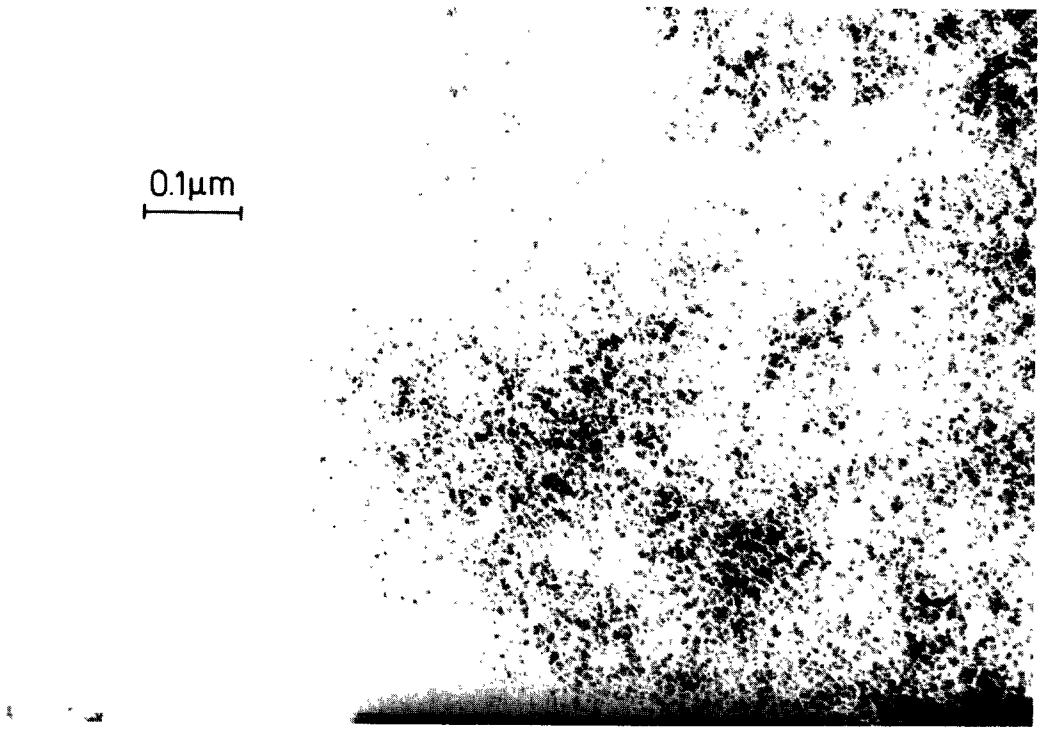

Fig. 2. Photograph of pulverized aerogel taken with a transmission electron-microscope [6].

The gel is prepared [2] from tetramethoxysilan, an ester of methanol and orthosilicic acid. It decomposes by hydrolyzation into both components. In a second step the silicic acid condenses into colloidal silica.

$$Si(OCH_3)_4 + 4H_2O \rightarrow Si(OH)_4 + 4CH_3OH \quad (2)$$

$$nSi(OH)_4 \rightarrow [SiO_2]_n + 2nH_2O. \quad (3)$$

If a catalyst, e.g. ammonia, is added the total reaction takes place in a reasonably short time. First the colloidal particles repell each other because of surface charges by ions of the catalyst. They may touch each other once they have grown to a sufficient size. Then they are bound together via unsaturated hydroxyl groups

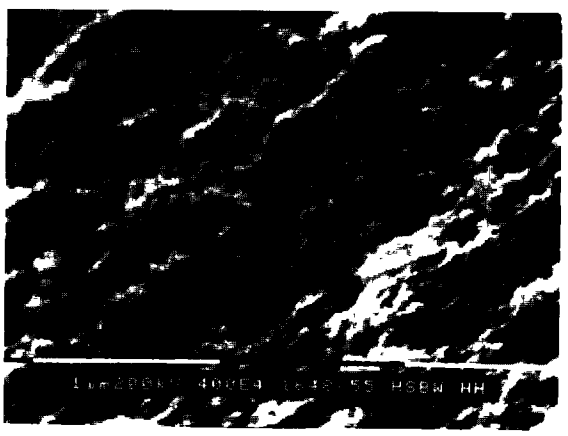

Fig. 3. Surface of a piece of aerogel photographed with a scanning electron-microscope [8]. The surface is covered with a layer of gold of about 5 nm.

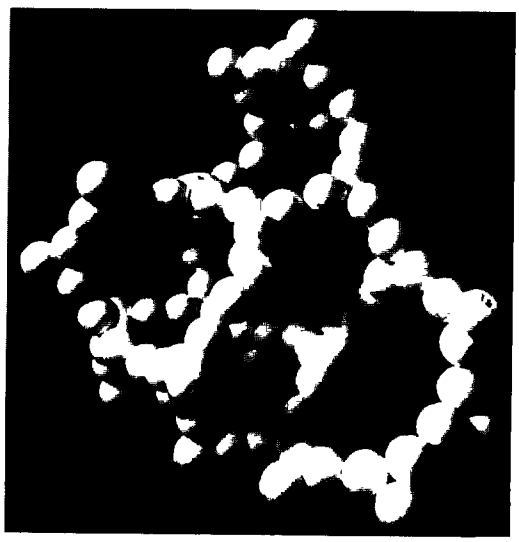

Fig. 4. Model of the structure of aerogel constructed according to Heesch and Laves [10]. In reality the particles have a diameter of about 40 nm and consist of clusters of silica colloides of about 4 nm in diameter. The particles are regularly packed with a coordination number of 3.

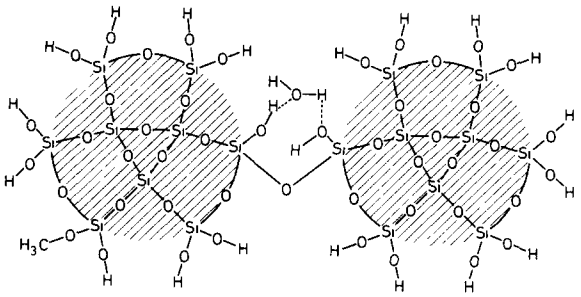

Fig. 5. Linkage of 2 silica colloides by a siloxan bond (Si–O–Si).

on the surface as demonstrated in fig. 5. In eq. (3) these hydroxyl groups have been neglected. A colloidal particle of 4 nm diameter, which contains 700 Si atoms and 400 OH-groups [9] should rather be described by $[SiO_2]_{700} \cdot [H_2O]_{400}$ or more precisely, equation (3) has to be replaced by

$$700\ Si(OH)_4 \rightarrow [(SiO_2)_{2\,5}\text{-}O\text{-}Si(OH)_2]_{200} + 1200\ H_2O. \quad (3a)$$

When almost all particles are linked together the substance forms a gel which occupies the same volume as the initial mixture. Hence, when methanol is added to the mixture the concentration of the silan and thus the density of the final gel is lowered. However, the gelling speed also decreases as the concentration of the silan is reduced as demonstrated in fig. 6. For a concentration by volume v_s below 0.1 no gellation is expected. Consequently, silica aerogels with refractivities $n - 1$ below 0.01 cannot be directly manufactured by this method.

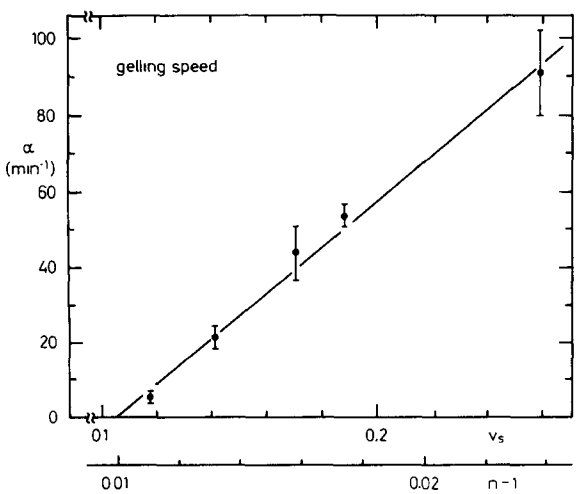

Fig. 6. Gelling speed normalized to unit concentration of catalyst (NH_4OH) as a function of the concentration of the silan. The corresponding refractivity of the final aerogel is also indicated.

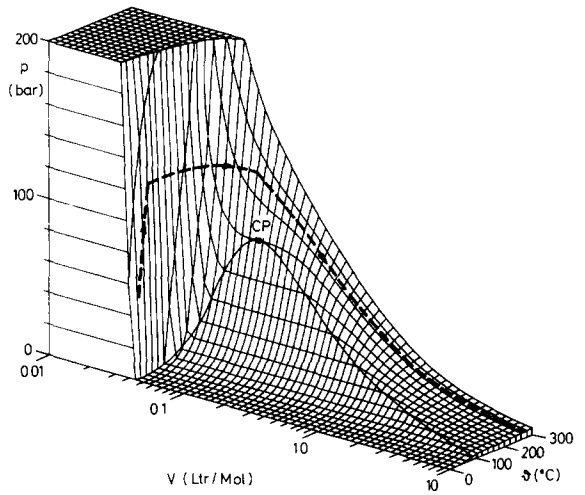

Fig. 7. Extraction cycle of methanol in the autoclave run (broken line) within the pressure–volume–temperature diagram for methanol. CP is the critical point.

The gel formed by reactions (2) and (3) still has methanol and water inside the pores. If it were simply dried, adhesion and capillary forces would contract the delicate structure. The liquid can be extracted without any harm when the gel is heated in a pressure vessel beyond the critical temperature (for methanol $\vartheta_c = 240°C$). After the critical point has been passed, the vapour can slowly be extracted. It is substituted by air when the pressure vessel is cooled down. The whole cycle is shown by the diagram in fig. 7, correlating pressure, volume and temperature for methanol and by its time dependence in fig. 8. The rates for the heating and for the subsequent extraction of the vapour are determined by the maximum allowable flux through the pores of the material. They can be derived from the viscosity of the methanol which decreases smoothly with temperature as can be seen in fig. 9 and by its thermal expansion. The expansion has to be taken into consideration more carefully as it is singular at the

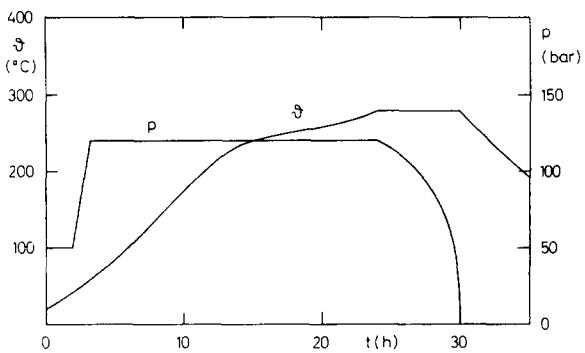

Fig. 8. Variation in time of temperature ϑ and pressure p in the autoclave

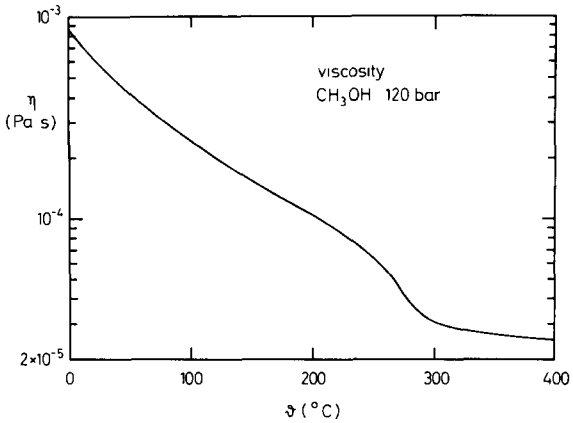

Fig. 9. Viscosity of methanol as a function of the temperature.

critical point (fig. 10). One chooses therefore an extraction cycle which keeps away from this singularity.

The freshly prepared aerogel still contains some residual methanol. Also the hydroxyl groups on the surface of colloidal particles have been replaced by methanol groups at the high temperature and pressure during the extraction cycle. It turns out that the optical properties improve when the alcohol is removed. For this purpose one heats the aerogel to 400°C in air. The methanol is thereby burned to formaldehyde and formic acid which readily escape. At the same time the physical character of the gel is changed. The initially hydrophobic aerogel is now hydrophilic.

The optical properties of aerogel are mainly determined by its granular structure. Fluctuations of the particle size and distribution lead to Rayleigh scattering of light. The mean scattering length increases as shown in fig. 11 with the 4th power of the wavelength [11]. In the visible range it amounts to about 3 cm. The absorption length is about 100 times longer, but it decreases

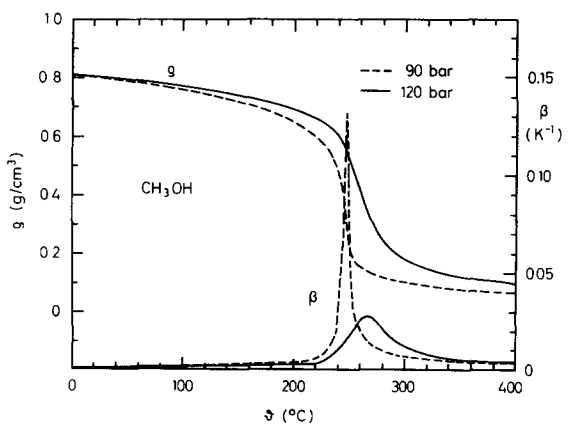

Fig. 10. Dependence of the density ρ of methanol on the temperature. Also drawn is the resulting thermal expansion coefficient β.

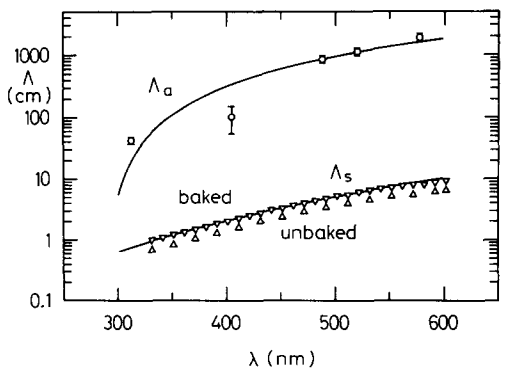

Fig. 11. Mean scattering length Λ_s for unbaked (Δ) and baked (∇) aerogel and mean absorption length Λ_a as a function of the wave length of light. The fit to the data for the scattering length behaves like $\lambda^{4\,0}$. The absorption length is fitted with a single resonance without damping.

quickly in the ultraviolet region. A one resonance fit to the absorption values indicates a resonance just below 300 nm. From data on the dispersion of aerogel given in table 1, one derives a resonance at $\lambda_0 = 90 \pm 50$ nm similar to silica glass. Absorbed gases will certainly lead to deviations. The transparency of aerogel improves if it is prepared with a high concentration of catalyst leading to short gelling times, as can be seen in fig. 12. With gelling times at 1°C of 12 min a transmission length at 436 nm of $\Lambda = 1/\mu = 5$ cm has been reached. The strong repulsion of the colloids force the particles to form a homogenous network.

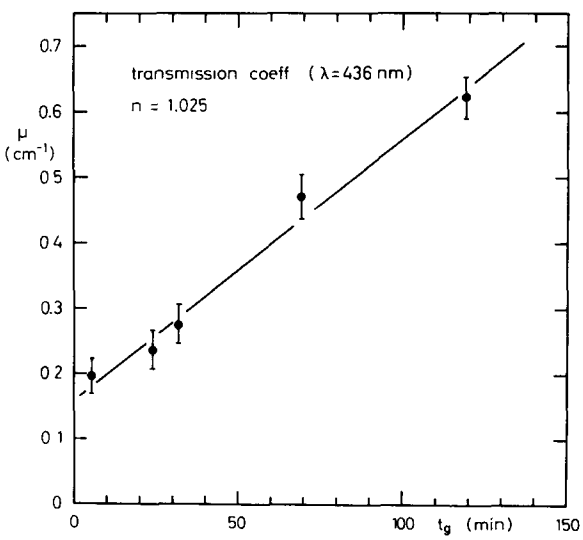

Fig. 12. Relation between the optical transmission coefficient μ of aerogel measured at λ = 436 nm and the gelling time t_g. The aerogel samples with an index of refraction of 1.025 were prepared with ammonia as catalyst. The lowest point was obtained at 1°C with $t_g = 12$ min. Its gelling time is rescaled to room temperature.

Table 1
Optical dispersion in Aerogel

Manufacturer	Sample	$n-1$ $\times 10^3$	λ (nm)	$n-1$ $\times 10^3$	λ (nm)	λ_0 (nm)
Bonn [12]	–	65 ±2	266	50 ±1	633	139± 7
DESY	1482	25.9±0.2	337	24.9±0.2	633	78±20
	1498	26.2±0.3	337	25.3±0.2	633	74±30
Airglass	a	21.2±0.2	337	20.3±0.2	633	82±25
	b	23.8±0.3	337	23.1±0.3	633	68±30

About 8000 liters of aerogel were manufactured at DESY during a development program and the following mass production. After the TASSO detector had been equipped the production was closed down.

3. Design of aerogel Cherenkov counters

In most of the existing Cherenkov counters, the light is collected by mirrors. Their optimum shape depends on the angular distribution of the incoming particles. In gas counters especially, paraboloidal or ellipsoidal mirrors are often used if the particles are in a parallel beam or come from a point-like source, respectively. The quality of the aerogel has reached such a high level, that such a design can also be adopted in the case of aerogel counters. A complication arises because of the larger Cherenkov angle. Large photomultipliers coupled to light collecting tubes are necessary to improve the acceptance. The detection efficiency of a counter is characterised by the mean number of photoelectrons $\langle N_e \rangle$ obtained. If the dependence of the various parameters on the wave length is neglected, one finds

$$\langle N_e \rangle = n_0 \sin^2\vartheta_c \cdot \Lambda (1 - e^{-d/\Lambda}), \tag{4}$$

where ϑ_c is the Cherenkov angle. The light collection is described by

$$n_0 = \frac{2\pi\alpha}{c} \Delta\nu \cdot \epsilon_{PM} \cdot \eta_m \cdot \eta_t. \tag{5}$$

The first terms with the fine structure constant α, the velocity of light c, the spectral response $\Delta\nu$ of the system and the efficiency ϵ_{PM} of the photomultiplier yield a factor of 90 cm^{-1} if a multiplier with a cathode efficiency of about 25% is used. The reflectivity η_m of a mirror can reach 0.9 and the transmission η_t of the tube is usually between 0.5 and 1.

The last factors in eq. (4) represent the effective thickness of the radiator of thickness d. If only direct unscattered light is collected the scattering length enters: $\Lambda = \Lambda_s$. For aerogel [13] available nowadays, with $\Lambda_s \approx 3$ cm, saturation is almost complete for a thickness $d \approx 3\Lambda \approx 9$ cm. With an index or refraction of $n = 1.025$ one obtains $\langle N_e \rangle \approx 10$.

If the aerogel samples are not perfect, e.g. if the surface is scratched or ground when cut by a saw, light collection by diffusely reflecting walls is recommended. Such a system is simple and easy to design. Eq. (4) is still valid, but in (5) η_m has to be replaced by the collection efficiency η_D of the diffusely reflecting walls of the detector box,

$$\eta_D = \frac{F_{PM}}{1 - \langle r \rangle (1 - F_{PM})}. \tag{6}$$

The mean reflectivity of the interior is given by

$$\langle r \rangle = F_D \cdot r_D + F_A \cdot r_A. \tag{7}$$

F_{PM}, F_D, F_A are the fractional areas of the photomultiplier window, of the diffuse reflector and of the aerogel respectively relative to the total internal area of the box and r_D, r_A are the corresponding reflectivities. Special filter papers [14] may be used as wall-papers because of their high reflectivity $r_D \approx 0.96$ and their own negligible yield of Cherenkov light. The reflectivity of the aerogel surface is calculated from diffusion theory [15] to be

$$r_A = \left(1 - 2\sqrt{\Lambda_s/3\Lambda_a}\right)/\left(1 + 2\sqrt{\Lambda_s/3\Lambda_a}\right) \approx 1 - 4\sqrt{\Lambda_s/3\Lambda_a} \approx 0.8, \tag{8}$$

where Λ_s and Λ_a are the scattering and the absorption length of aerogel respectively.

One obtains $\eta_D = 0.1$ for large and 0.3 for small boxes. The effective length in eq. (4) is now given by the diffusion length Λ_D

$$\Lambda = \Lambda_D = \sqrt{\Lambda_s \cdot \Lambda_a/3} \approx 15 \text{ cm}. \tag{9}$$

For a saturated counter ($d \approx 45$ cm) one obtains again $\langle N_e \rangle \approx 10$ photoelectrons. The light path in diffusely reflecting boxes is rather long. This results in a mean light collection time given by

$$\langle \tau \rangle = -\langle l \rangle \left(c \cdot \ln\left[(1 - F_{PM})\langle r \rangle\right]\right)^{-1}, \tag{10}$$

where $\langle l \rangle$ is the mean free path of the light. For the TASSO Cherenkov counters [4] one has $\langle l \rangle \approx 64$ cm, resulting in

$\langle \tau \rangle \approx 25$ ns.

Cherenkov counters of the diffuse reflection type are characterized by their homogeneous response but they

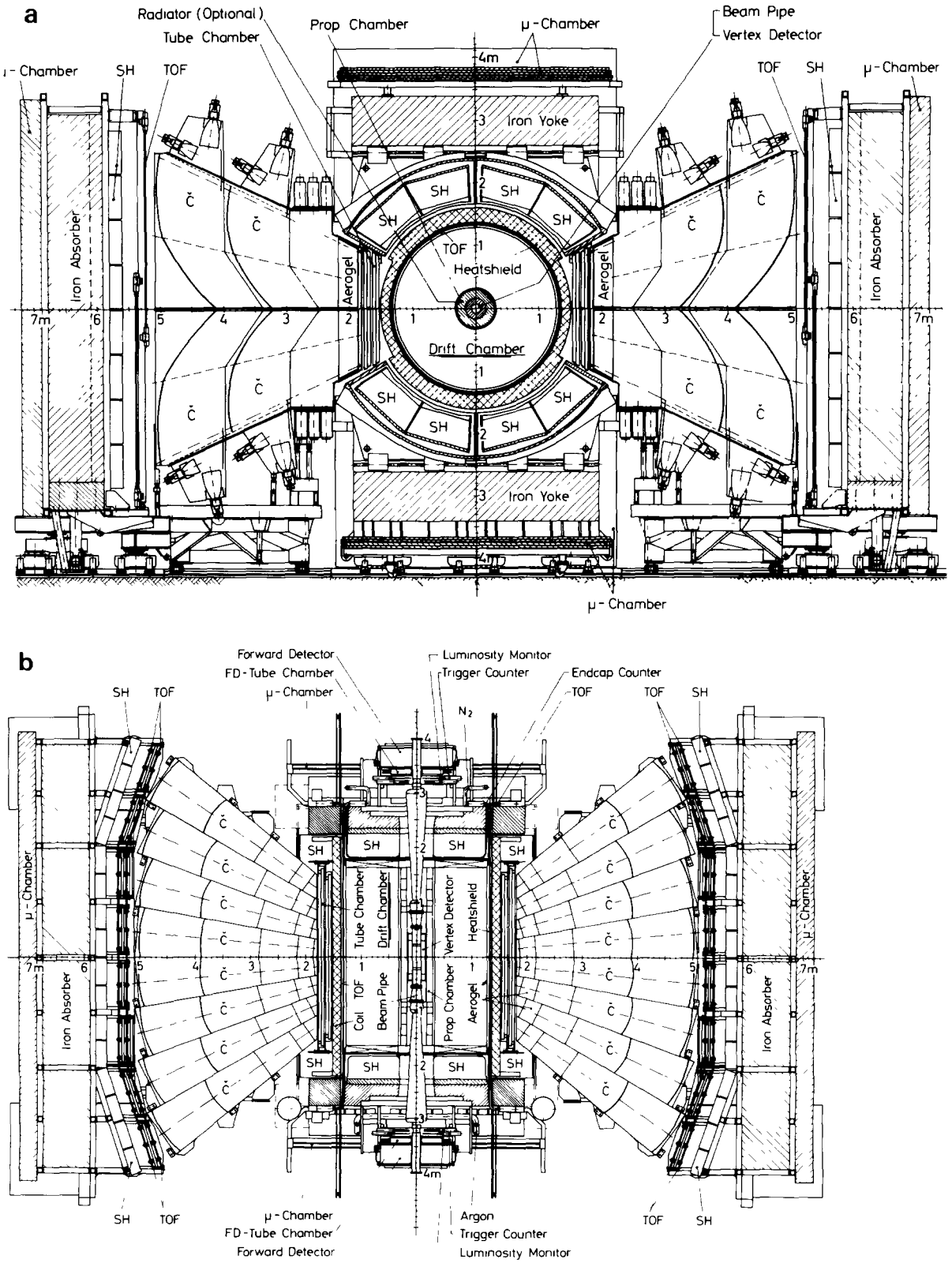

Fig. 13. Front and top view of the TASSO detector. C, TOF and SH are Cherenkov-, time-of-flight and shower counters respectively.

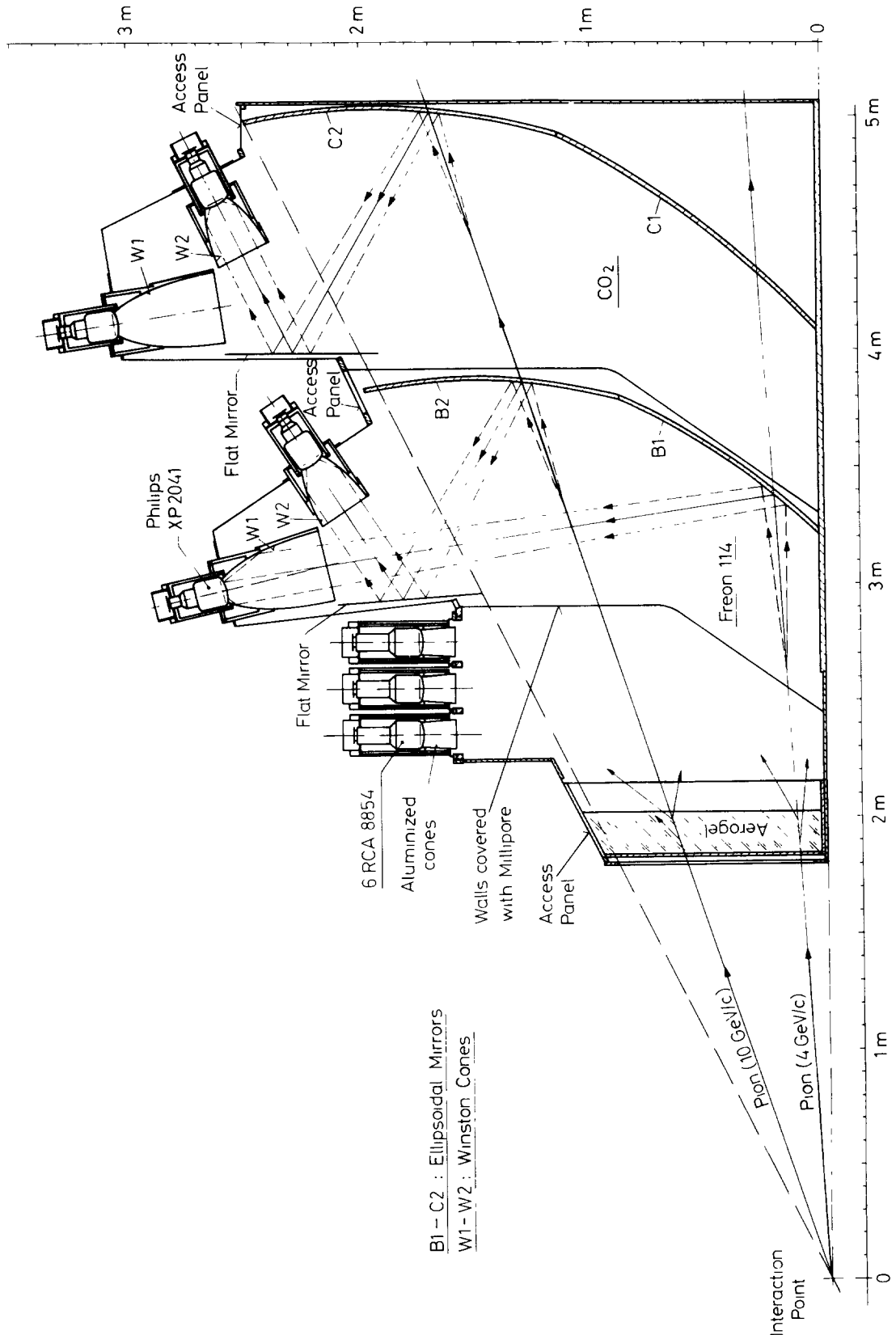

Fig. 14. Light collection system for the aerogel and the 2 gas Cherenkov-counters in one TASSO arm.

are sensitive to particles entering from any direction. Other light collection systems are also possible. A hybrid system of both schemes with a thick aerogel layer and with mirrors is being operated at CERN [16]. Wavelength shifter readout is also possible [17].

4. Aerogel Cherenkov counters in TASSO

The two "hadron arms" of the TASSO detector at the PETRA storage ring at DESY are equipped with large Cherenkov counters [4] used to identify particles form e^+e^- interactions. Schematic drawings of the detector are shown in figs. 13a and 13b. The operation of the Cherenkov counters is seen in more detail in fig. 14 (see also table 2). Two gas counters, filled with Freon 114 and CO_2 respectively are placed behind the aerogel counters. In each gas cell the light is collected by 2 different ellipsoidal mirrors with the interaction point at the one focus and a photomultiplier at the second one.

The radiator of an aerogel cell has a cross section of 100×35 cm^2. It consists of several layers of aerogel slabs $17 \times 17 \times 2.3$ cm^3 each, cut by a diamond saw to the appropriate shape. The entire box is lined with millipore paper. The 6 photomultipliers with 5 in. windows are of the quantacon type, and are able to detect single photoelectrons. The light yield was measured with a prototype cell filled with aerogel of $n = 1.024$ exposed to a beam of relativistic pions (fig. 15). The yield was found to increase with the thickness d of the aerogel according to a diffusion length $\Lambda_D = 9$ cm. Later measurements [18] with cosmic muons and with aerogel of higher quality yielded 10% more light (open circle in fig. 15). With aerogel of $n = 1.017$ a thickness of 23 cm is necessary to obtain 3.9 ± 0.3 photoelectrons (full square). The higher quality of this aerogel ($\Lambda_s = 3.8$ cm at $\lambda = 436$ nm) was compensated by the lower number of intrinsic Cherenkov photons. If the walls of the counter were covered with aluminized mylar, and an appropriately bent foil was put opposite the aerogel, the photoelectron yield decreased to 3.1 ± 0.1 (open square). Such large detectors are not so well suited for light collection by mirrors. Monte Carlo calculations showed

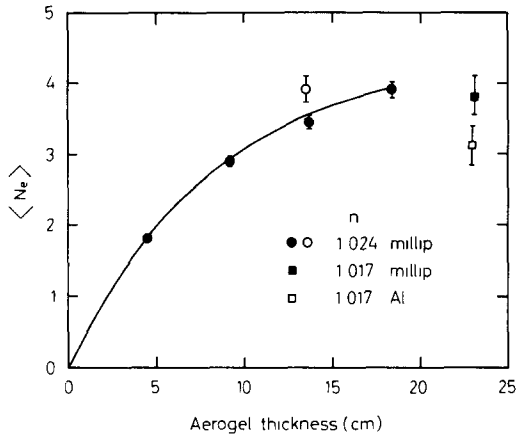

Fig. 15. Mean photoelectron yield of one aerogel cell of TASSO for different radiator thickness. The data were taken in a pion beam of 3.4 GeV/c and with cosmic muons. The open point is the mean value obtained with 16 TASSO cells. Test results (squares) with aerogel having $n = 1.017$ and light collection by diffuse reflection (■) and via aluminized mylar (□) are also shown.

that highly sophisticated mirror shapes would be necessary.

The response of the counter was rather uniform. The photoelectron yield varied smoothly within $\pm 20\%$ along the 1 m counter length.

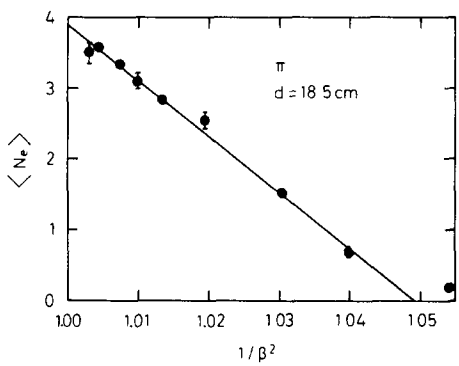

Fig. 16. Threshold curve of a TASSO aerogel cell in a pion beam.

Table 2
Cherenkov system of the TASSO detector.
Total system: Front face 11.8 m^2 ($\vartheta = 90° \pm 40°$, $\varphi_1 = \pm 26°$, $\varphi_2 = 180° \pm 26°$). Solid angle $\Delta\Omega/4\pi = 19\%$.

System	Number of cells	Radiator		Index of refraction	Granularity		$\langle N_e \rangle$ for $\beta = 1$ particles
		volume (l)	thickness (cm)		$\Delta\vartheta$	$\Delta\varphi$	
Aerogel	32	1700	13.5– 18	1.024 ± 0.002	10°	26°	4
Freon 114	64		80 –100	1.0014	10°	13°	20
CO_2	64		90 –120	1.00043	10°	13°	8

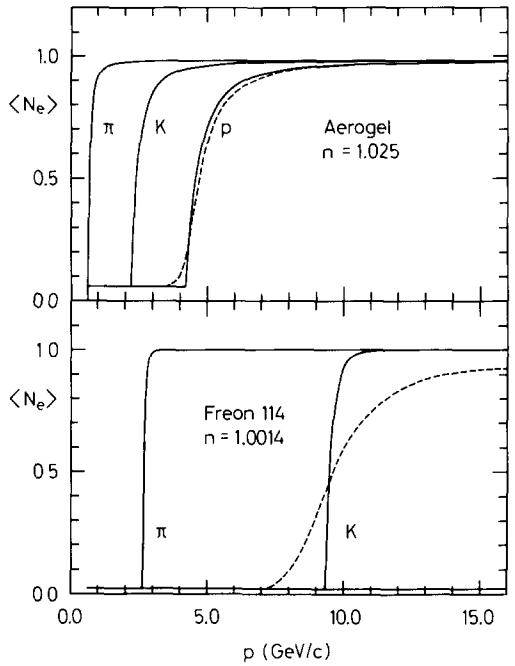

Fig. 17. Calculated momentum thresholds for the aerogel and Freon 114 counters of TASSO for pions, kaons and protons. The dashed lines indicate the influence of the finite momentum resolution of $\sigma_p/p = 1.7\sqrt{1+p^2}\,\%$ of the TASSO inner detector.

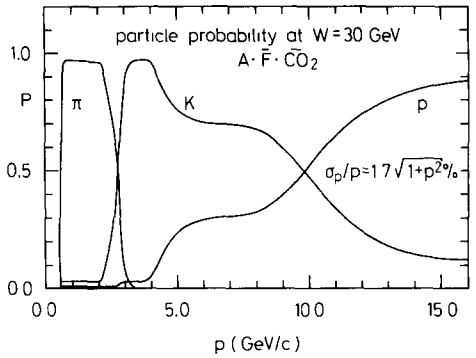

Fig. 18. Probability for a coincidence of the type (aerogel·$\overline{\text{Freon}}$·$\overline{CO_2}$) to signal a pion, kaon or proton as a function of the particle momentum.

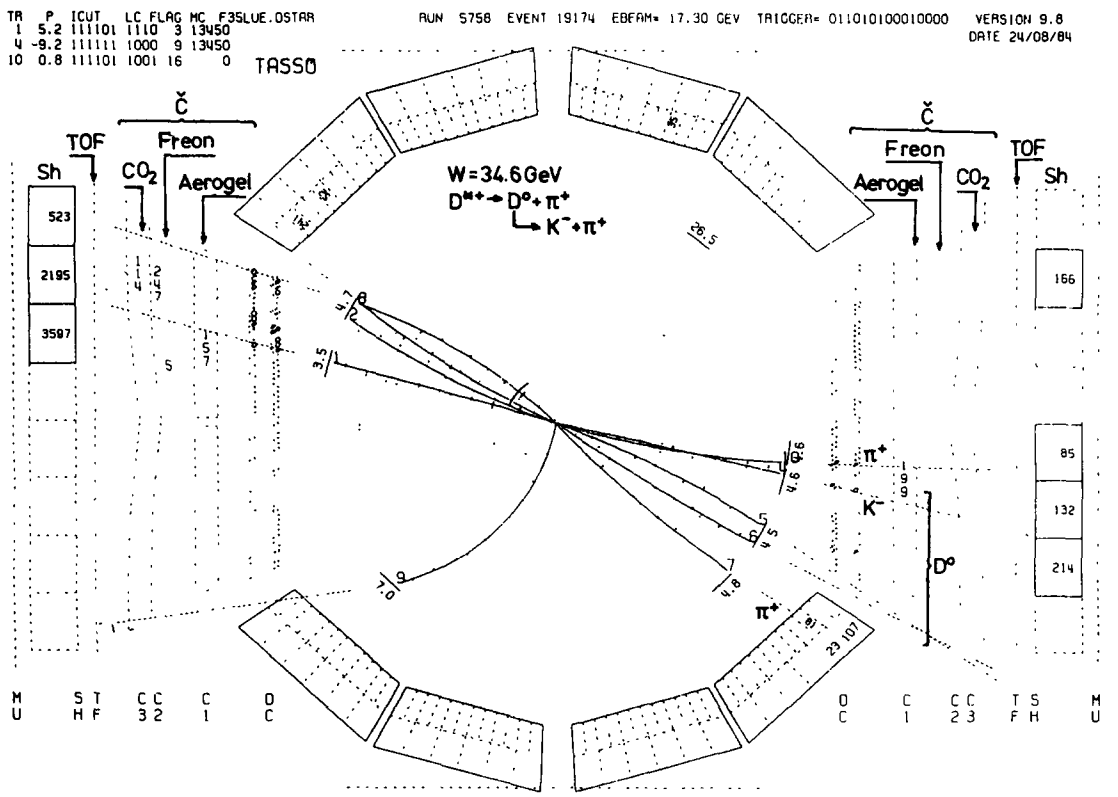

Fig. 19. Reconstruction of an e^+e^- annihilation at 34.6 GeV cm energy. A D^{*+} is produced which decays into a π^+ and a D^0, which in turn decays into a K^- and a π^+. The K^- (9.2 GeV/c) and one π^+ (0.8 GeV/c) are identified by the Cherenkov system, by triggering separate aerogel counters but no gas counter.

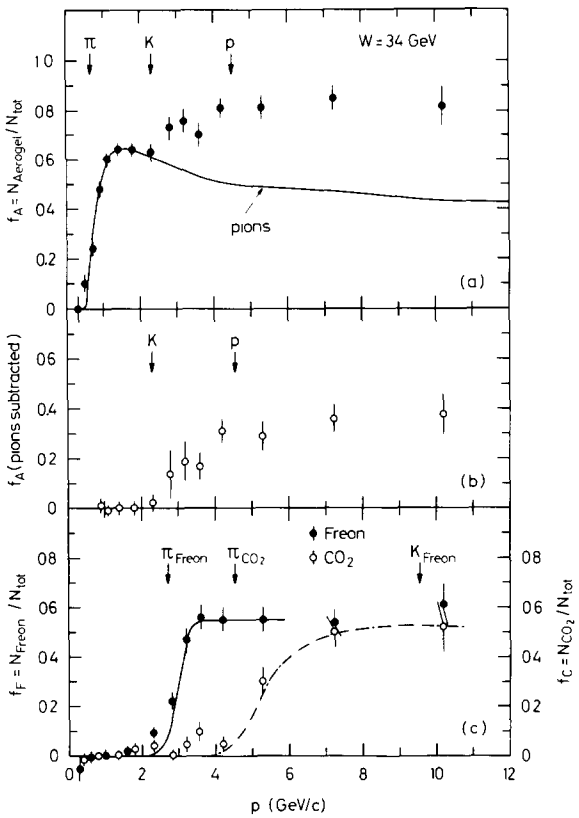

Fig. 20. (a) Fraction of particles f_A from multihadronic events which produce light in the aerogel counters of TASSO versus the particle momentum. (c) The corresponding fractions f_F and f_C for the Freon and CO_2 counters respectively.

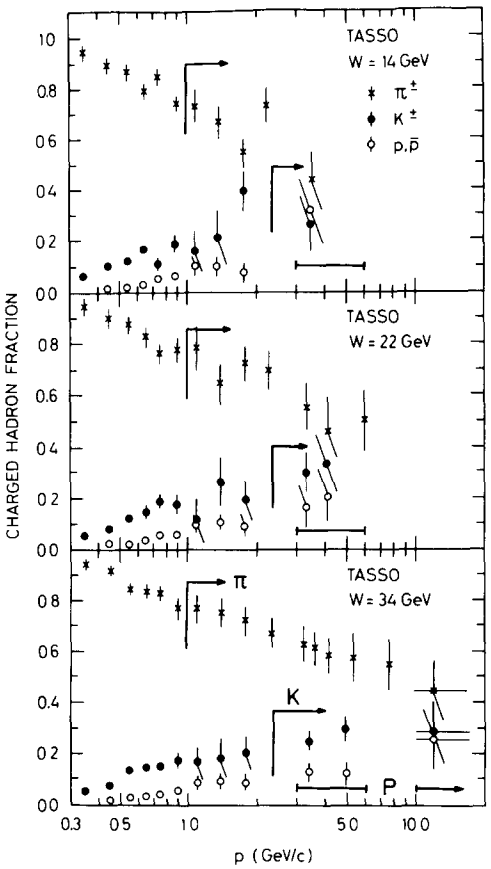

Fig. 21. Fraction of charged π, K and protons in an event computed from the data in fig. 20 and from TOF data. The arrows show the range of the Cherenkov system.

The threshold curve measured with pions shows the expected behaviour (fig. 16). The background of 0.06 photoelectrons below threshold is mainly caused by knock-on electrons produced in the material upstream and in the aerogel itself.

To obtain the information on the nature of the particles the signals from the aerogel and from both gas counters in the TASSO detector are combined. The calculated threshold curves for the aerogel and the Freon 114 counters are shown in fig. 17. If the momentum resolution of $\sigma/p = 1.7(1+p^2)^{1/2}\%$ (p in GeV/c) is included the thresholds of response beyond 5 GeV/c are expanded quite substantially. For one of the combinations, namely a signal in the aerogel in anticoincidence with Freon and CO_2 counter signals, the probabilities for a track to be a pion, kaon or proton is shown in fig. 18. It exhibits a weakened discrimination between kaons and protons at high momentum caused by the finite momentum resolution.

An e^+e^- annihilation event at 34.6 GeV cm energy observed in the TASSO detector is presented in fig. 19 after computer reconstruction. A D^{*+} is produced, which subsequently decays into a π^+ and a D^0 which in turn decays further to K^- and π^+. The kaon with a momentum of 9.2 GeV/c and one π^+ (0.8 GeV/c) yield signals in different aerogel counters but not in the gas counters. Thus both particles can be identified. In fig. 20a the fraction f_A of all tracks that produced light in the aerogel counters is plotted versus the momentum of the particles [19]. The pion threshold is evident. If the pions are subtracted (fig. 20b) the kaons and protons remain. In fig. 20c the fractions of all tracks that produced light in the gas counters are shown. After corrections for acceptance, background, counter inefficiency etc, the Cherenkov data and the data from the time-of-flight counters (TOF) yield the fractions of $\pi/K/p$ among the charged hadrons (fig. 21). The arrows in the figure indicate the momentum range of the Cherenkov system. It well overlaps with the range of the TOF counters.

The inclusive cross sections also demonstrate the analysing power of the Cherenkov system. The kinematically accessible region of the pion momentum is almost fully covered by the Cherenkov system (fig. 22). The kaons and protons are produced with lower cross sections and their spectra are shifted to low velocities.

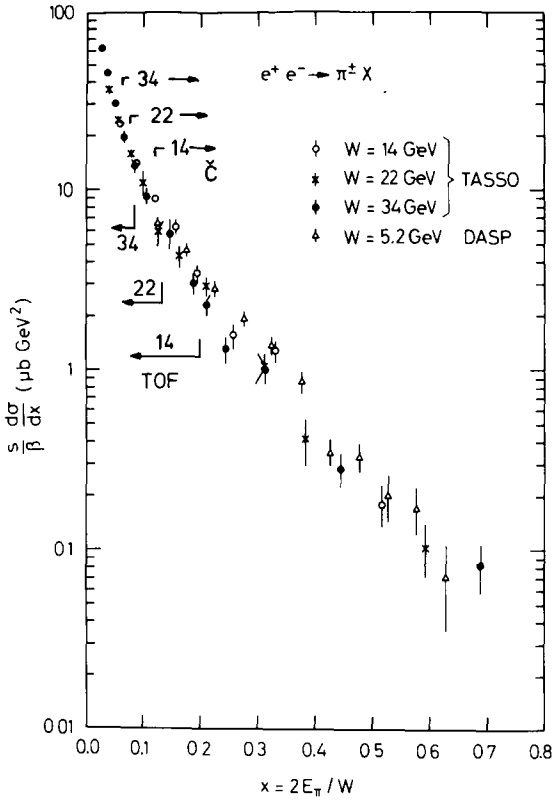

Fig. 22. Inclusive pion cross section as a function of the relative pion energy. The range of the Cherenkov and the TOF system are indicated.

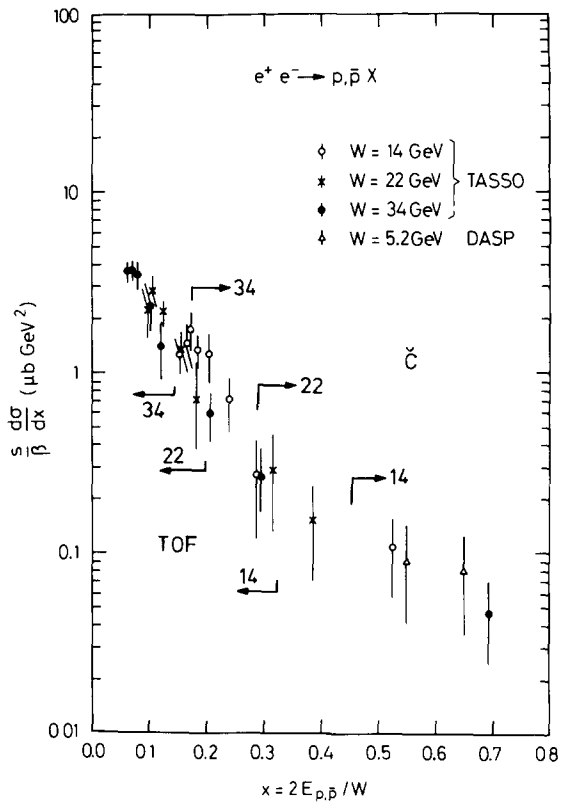

Fig. 23. Cross section of inclusively produced protons; x is the particle energy normalized to the beam energy.

Thus the Cherenkov data suffer from low statistics. In addition, a gap in the K/p-separation ability exists between 6 and 10 GeV/c because of the threshold positions of the aerogel and freon counters. Nevertheless, the data in fig. 23 show that the system is also able to extend the TOF range to higher x values for protons.

5. Long term behaviour of aerogel Cherenkov counters

Fig. 24 shows [20] that during the 4 years of operation the photoelectron yield steadily dropped to 50% of its original value. The slope is -0.5 photoelectrons/yr. In spite of constant flushing with dry nitrogen, organic vapours from paints and glues were absorbed by the porous aerogel which became yellowish or even brown. Especially slabs deposited close to double sticky tapes were strongly affected. When the aerogel in one cell was replaced by new samples [21] the light yield recovered to 85% of its original value. When the millipore paper was also exchanged the initial efficiency was obtained. Similar effects have been reported from the EHS detector [16]. The open points in fig. 24 suggest an exponen-

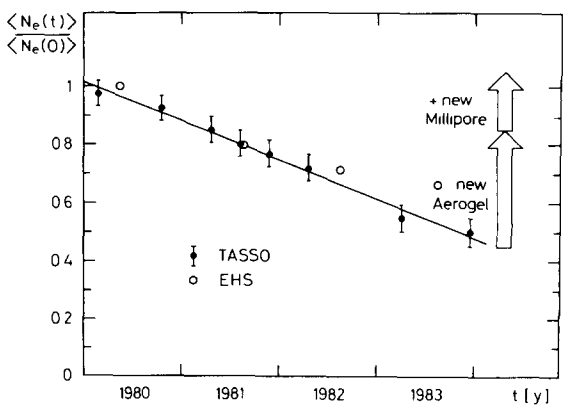

Fig. 24. Photoelectron yield of the TASSO aerogel counters for relativistic particles along the time of operation. The yield decreases with a slope of 0.5 yr^{-1}. The arrows show the improvement obtained when new aerogel and new millipore was recently installed in one cell. The data from the EHS detector [16] indicate a similar decrease but suggest an exponential decay with a time constant of 7.5 yr.

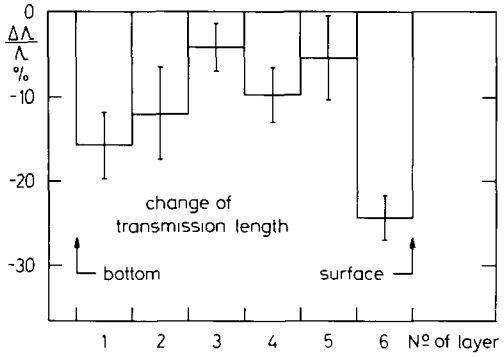

Fig. 25. Relative change in transmission length of aerogel samples after 4 yr of installation in the TASSO aerogel counters. The aerogel slabs were placed in the counter in 6 layers.

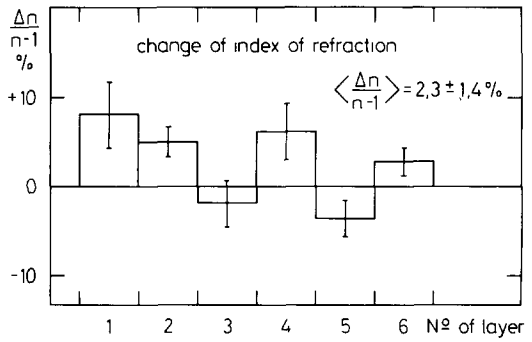

Fig. 26. Relative change in the refractivity of the same samples, described in fig. 25.

tial decrease with a time constant of 7.5 yr.

A detailed investigation of the 6 layers in the TASSO aerogel cells showed a strong decrease in the transmission length of the bottom layer (closest to the paint) and of the top layer by 15% and 25% respectively (fig. 25). The pieces are still transparent but the change in colour indicates that the reduction in the transmission length is dominated by a decrease in the absorption length by 78% (from 200 to 45 cm at 400 nm) and the scattering length by about 7.5%. This reduces the effective thickness of the aerogel via eq. (9) and its reflectivity (eq. (8)). The reflectivity of the millipore paper must be dropped in addition from 96 to 94%.

The change in the refractivity is plotted in fig. 26. It is slightly positive, but still compatible with zero.

The construction of aerogel Cherenkov-counters keeping a constant efficiency over many years of operation should not be difficult. The housing has only to be gas tight and should not contain any outgasing material. This would not affect the advantages of such an instrument. The walls can still be thin and the construction is still uncomplicated.

References

[1] A. Linney and B. Peters, Nucl. Instr. and Meth. 100 (1972) 545.
[2] M. Cantin, M. Casse, L. Koch, R. Jouan, P. Mestreau, D. Roussel, F. Bonnin, J. Moutel and S.J. Teichner, Nucl. Instr. and Meth. 118 (1974) 177.
[3] G. Poelz and R. Riethmüller, Nucl. Instr. and Meth. 195 (1982) 491.
[4] H. Burkhardt, P. Koehler, R. Riethmüller, B.H Wiik, R. Fohrmann, J. Franzke, H. Krasemann, R. Maschuw, G. Poelz, J. Reichardt, J. Ringel, O. Römer, R. Rüsch, P. Schmüser, R. van Staa, J. Freeman, P. LeComte, T. Meyer, Sau Lan Wu, and G. Zobernig, Nucl. Instr. and Meth. 184 (1981) 319.
[5] S. Henning and L. Svensson Phys. Scripta 23 (1981) 697.
[6] The microphotograph was taken by M. Harsdorff and I. Nack, Inst. für Angewandte Physik der Universität Hamburg, Germany.
[7] G. Nicolaon, Contribution à l'étude des aerogels de silices, Thesis, University of Lyon (1968).
[8] The photograph was taken by H. Kreye and K. Müller, Hochschule der Bundeswehr, Hamburg.
[9] R.K. Iler, The colloid chemistry of silica and silicates (Cornell University, Ithaca, NY, 1955).
[10] H. Heesch and F. Laves, Z. Kristallogr. A85 (1933) 443.
[11] J. Reichardt, Aerogel-Cherenkovzähler für TASSO, Thesis, II. Inst. für Experimentalphysik der Universität Hamburg (1980).
[12] U. Hartfiel, Bau und Test eines Aerogel-Cherenkov-Zählers. Thesis, Bonn-IR-79-46 (1979).
[13] G. von Dardel and S. Henning, Airglass AB, Sjöbo, Sweden.
[14] Filter paper GS from Millipore Corporation Bedford, MA, USA or OE66 from Schleicher & Schüll GmbH, Dassel, Germany.
[15] S. Glasstone and M.C. Edlund, The elements of nuclear reactor theory (Princeton, 1952 and Springer, Wien, 1961).
[16] P.J. Carlsson, these Proceedings, A248 (1986) 110.
[17] S. Henning, G. Jarlskog, U. Mjörnmark, A. Nilsson and L. Svensson, Phys. Scripta 23 (1981) 703.
C. Aurouet, H. Blumenfeld, M. Bourdinaud, C. Jeanney, C. Lafond and C. Perrin, Nucl. Instr. and Meth. 211 (1983) 309.
[18] TASSO Collaboration R. Brandelik et al., Phys. Lett. 113B (1982) 98.
[19] TASSO Collaboration M. Althoff et al. Z. Phys. C 17 (1983) 5.
[20] H. Krasemann, thesis, II. Inst. für Experimentalphysik der Universität Hamburg (1985).
[21] New aerogel was bought from Airglass AB [13].